

Nonordinary edge criticality of two-dimensional quantum critical magnets

Lukas Weber,¹ Francesco Parisen Toldin,² and Stefan Wessel¹

¹*Institut für Theoretische Festkörperphysik, JARA-FIT and JARA-HPC,
RWTH Aachen University, 52056 Aachen, Germany*

²*Institut für Theoretische Physik und Astrophysik,
Universität Würzburg, Am Hubland, 97074 Würzburg, Germany*

(Dated: November 6, 2018)

Based on large-scale quantum Monte Carlo simulations, we examine the correlations along the edges of two-dimensional semi-infinite quantum critical Heisenberg spin-1/2 systems. In particular, we consider coupled quantum spin-dimer systems at their bulk quantum critical points, including the columnar-dimer model and the plaquette-square lattice. The alignment of the edge spins strongly affects these correlations and the corresponding scaling exponents, with remarkably similar values obtained for various quantum spin-dimer systems. We furthermore observe subtle effects on the scaling behavior from perturbing the edge spins that exhibit the genuine quantum nature of these edge states. Our observations furthermore challenge recent attempts that relate the edge spin criticality to the presence of symmetry-protected topological phases in such quantum spin systems.

Quantum criticality in quantum many-body systems is a central aspect of current research in condensed matter physics [1]. In this respect, quantum spin systems in particular allow for a detailed comparison of experimental results to a quantitative computational modeling and analytical calculations of critical properties. Prominent examples are dimerized antiferromagnets, in which an explicit dimerization of the exchange couplings can be varied (e.g., by applying pressure [2–5]) in order to induce quantum phase transitions between quantum disordered phases and conventional antiferromagnetic order. In the absence of frustration, the quantum critical properties of such systems in d spatial dimensions are generally considered to be in accord with the universality class of the $(d + 1)$ -dimensional classical Heisenberg model at its finite temperature critical point, described by the Wilson-Fisher fixed point of the three-component ϕ^4 theory [6]. This rationale is supported also by large-scale numerical studies of coupled spin dimer models on various two-dimensional (2D) lattices [1, 7, 8, 10–12]. Within the nonlinear σ -model description of quantum antiferromagnets [13–21], such an agreement with the critical ϕ^4 theory suggests that for this purpose spin Berry-phase contributions [22] can be neglected in the effective action for 2D dimerized quantum antiferromagnets [21] (they may however give rise to additional scaling corrections from cubic terms in coupled dimer systems with reduced spatial symmetries [23]). As is well known, this is in stark contrast to the one-dimensional (1D) Heisenberg spin-1/2 chain, for which uncompensated spin Berry phases lead to a nonvanishing topological θ -term in the effective continuum action, associated with a gapless, quantum critical ground state [13–18]. Such a topological term can also emerge for a one-dimensional edge of 2D quantum spin systems: by appropriately cutting a 2D quantum antiferromagnet to a semi-infinite system, an effective 1D edge spin-1/2 system with similarly uncompensated Berry phases is generated. Such edge spins are further-

more susceptible to effective interactions induced by the coupling of the edge spins to the bulk. If the bulk system resides within the quantum disordered region, these effective interactions along the edge spins decay exponentially over a length scale set by the finite bulk correlation length. Due to the bipartite lattice structure, they respect a bipartite alignment of the edge spin chain, and thereby lead to long-distance ground state correlations as in a spin-1/2 Heisenberg chain (see Supplemental Material [24]). The presence of such gapless edge states of dimerized bulk systems was furthermore found to be stable against various perturbations [25], whereas the scaling properties were found to strongly depend on the model parameters and the nature of the applied perturbation [25].

Here, we consider edge spin systems for which the bulk itself is tuned onto a quantum critical point: the long-ranged quantum critical bulk fluctuations then dominate the effective interactions among the edge spins, which effects changes in the scaling properties of the correlations along the edge. As for bulk criticality, one may consider a comparison to surface critical phenomena in classical systems, for which several scenarios can be distinguished regarding the bulk vs surface critical behavior [26–28]. In addition to the ordinary transition, at which the surface is critical due to the bulk transition, the surface may also order at a higher temperature scale than the bulk. Such a surface transition typically requires enhanced interactions at the surface with respect to those of the bulk, in order to compensate for the reduced coordination along the surface. At the bulk transition temperature, the ordered surface may in this case still exhibit additional singular behavior, known as the extraordinary transition. One may furthermore fine-tune the surface coupling to a multi-critical special transition, at which surface and bulk are critical simultaneously. Based on the quantum-to-classical correspondence, one would expect the edge spins of a semi-infinite quantum critical

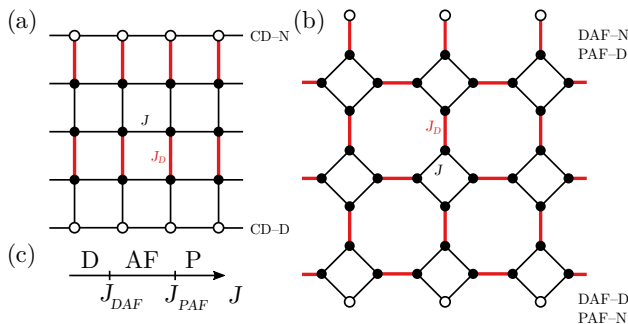


FIG. 1. (Color online) (a) CD lattice with an edge of dangling spins shown on the bottom edge (CD-D) and nondangling spins on the top edge (CD-N). (b) PS lattice with dangling (nondangling) edge spins on the bottom (top) edge, for the DAF-D and DAF-N cases, respectively, and with dangling (nondangling) edge spins on the top (bottom) edge, for the PAF-D and PAF-N cases, respectively. In both panels, the interdimer (intra-dimer) couplings J (J_D) are indicated by black (bold red) lines, the edge (bulk) spins by open (full) symbols, and periodic boundary conditions by open lines. (c) Phase diagram of the PS lattice with the antiferromagnetic region (AF), the dimer phase (D) for $J < J_{DAF} \approx 0.6J_D$, and the plaquette phase (P) for $J > J_{PAF} \approx 1.1J_D$.

spin system to similarly exhibit genuine quantum critical behavior. However, it should be noted that a $SU(2)$ -symmetric 2D quantum system corresponds to a 3D classical Heisenberg system with $O(3)$ symmetry, for which a 2D surface may not order at finite-temperatures [29], in contrast to the generic scenario outlined above. Instead, it has been suggested that in this case the surface may exhibit a Kosterlitz-Thouless transition upon varying the surface coupling [30]. A direct analogy to the classical case is furthermore exacerbated by the fact that for a 2D quantum spin system additional terms to the effective action from the Berry phases of the edge spins may affect the critical properties in subtle ways. Below we provide evidence that this is indeed the case. For this purpose, we examined several specific coupled spin-dimer systems that are described by a generic Hamiltonian $H = J \sum_{\langle i,j \rangle} \mathbf{S}_i \cdot \mathbf{S}_j + J_D \sum_{\langle i,j \rangle_D} \mathbf{S}_i \cdot \mathbf{S}_j$, where the first (second) term contains the interdimer (intradimer) couplings of strength J (J_D) of different geometries, to be specified below (we fix $J_D = 1$). We performed quantum Monte Carlo (QMC) simulations of such coupled spin-dimer systems using the stochastic series expansion [31] approach with deterministic operator loop updates [32, 33]. For a 2D system, the number of spins scales as L^2 with the linear system size, and in order to probe ground state properties we scaled the temperature as $T = 1/(2L)$, respecting the dynamical critical exponent $z = 1$ for the bulk transition. In the following, we present the QMC results for various edge configurations.

We first consider the columnar-dimer (CD) lattice shown in Fig. 1(a). Its bulk quantum critical point has

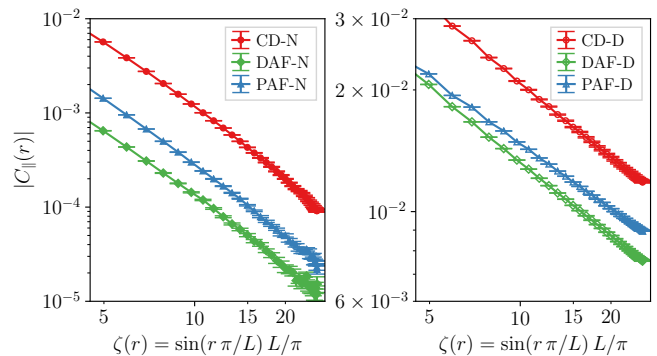


FIG. 2. (Color online) $C_{\parallel}(r)$ vs. $\zeta(r) = \sin(r\pi/L)L/\pi$ for the different edge spin configurations shown in Fig. 1.

been located previously at $J = 0.52337(3)$ [8, 10]. Using periodic boundary conditions (PBC) along the lattice direction parallel to the dimers, we examine separately the two cases of cutting along the perpendicular direction, obtaining either an edge of dangling spins (with respect to the J_D bonds), denoted CD-D, or an edge of nondangling spins, denoted CD-N cf. Fig. 1(a). For both cases, we performed QMC simulations to measure the spin-spin correlations $\langle S_i^z S_j^z \rangle$ among two edge spins i, j at a distance r parallel to the edge, denoted $C_{\parallel}(r)$, as well as between an edge spin i and an equivalent bulk spin j (with respect to the unit cell) at a distance r perpendicular to the edge, denoted $C_{\perp}(r)$. In addition, we also accessed the staggered susceptibility χ_s of the edge spin subsystem from the Kubo integral [31], $\chi_s = \frac{1}{L} \int_0^\beta d\tau \langle M_s(\tau) M_s(0) \rangle$, of the staggered edge moment $M_s = \sum_i' \varepsilon_i S_i^z$, where the summation is restricted over the edge spins ($\varepsilon_i = \pm 1$ depending on the sublattice to which site i belongs). The resulting data for $C_{\parallel}(r)$ on a $L = 80$ system is shown (along with that for several other cases, discussed below) in Fig. 2. It shows $C_{\parallel}(r)$ as a function of the conformal length (cord distance) $\zeta(r) = \sin(r\pi/L)L/\pi$, to account for the PBC along the edge. For both cases, we observe an approximately algebraic decay, indicative of a quantum critical state of the edge spin system that can be quantified by the scaling $|C_{\parallel}(r)| \propto r^{-z-\eta_{\parallel}}$, with an anomalous critical exponent η_{\parallel} and with $z = 1$, here and in the following. The drop of the correlation functions at large values of $\zeta(r)$, explicitly seen in the weaker-correlated nondangling case, indicates residual finite-size effects (see Supplemental Material [24]). To account for finite-size corrections, we estimate η_{\parallel} from the finite-size scaling of $C_{\parallel}(L/2)$ vs L as $C_{\parallel}(L/2) = (L/2)^{-z-\eta_{\parallel}}(c_0 + c_1 L^{-\omega})$, including a subleading scaling correction (in practice, we fix $\omega = 1$ [12, 24]), and c_0 and c_1 as nonuniversal fit parameters. We obtain this way the estimates $\eta_{\parallel} = -0.50(1)$ (CD-D) and $\eta_{\parallel} = 1.30(2)$ (CD-N), respectively, cf. Table I and the scaling plots in the top panel of Fig. 3. We also observe scaling for $C_{\perp}(L/2)$ (cf. Fig. 3), and from a

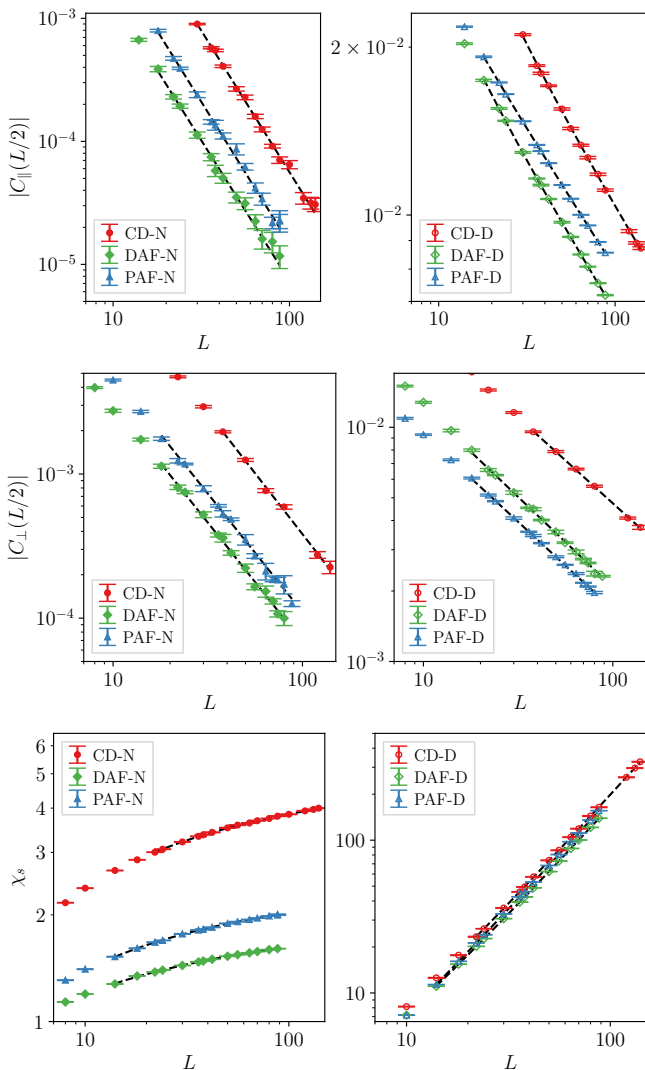


FIG. 3. $C_{\parallel}(L/2)$ (top panels), $C_{\perp}(L/2)$ (middle panels), and χ_s (bottom panels) as functions of L for the different configurations of Fig. 1 along with finite-size fits (dashed lines).

corresponding fit to $C_{\perp}(L/2) = (L/2)^{-z-\eta_{\perp}}(c_0 + c_1 L^{-\omega})$ obtain the estimates for η_{\perp} provided in Table I (see Supplemental Material [24]). Furthermore, from the finite-size scaling $\chi_s \sim L^{-(1+z-2y_{h_1})}$, we estimate the scaling dimension y_{h_1} of the (staggered) field along the edge. With $z = 1$, this scaling corresponds to the standard form for classical surface critical behavior [26–28] for a 3D bulk system in terms of the surface field scaling dimension y_{h_1} , and for which the following scaling relations hold: $\eta_{\parallel} = 3 - 2y_{h_1}$, $2\eta_{\perp} = \eta_{\parallel} + \eta$. Here, η is the anomalous dimension at the bulk transition, with $\eta = 0.0375(5)$ for the 3D $O(3)$ universality class [34]. We can estimate y_{h_1} from the QMC data based on the finite-size scaling form $\chi_s = c_{ns} + L^{-(1+z-2y_{h_1})}(c_0 + c_1 L^{-\omega})$ that includes an additive constant c_{ns} to account for regular contributions in the nondangling case (see Supplemental Ma-

Configuration	η_{\parallel}	η_{\perp}	y_{h_1}
CD-N	1.30(2)	0.69(4)	0.84(1)
DAF-N	1.29(6)	0.65(3)	0.832(8)
PAF-N	1.33(4)	0.65(2)	0.82(2)
CD-D	-0.50(1)	-0.27(1)	1.740(4)
DAF-D	-0.50(1)	-0.228(5)	1.728(2)
PAF-D	-0.517(4)	-0.252(5)	1.742(1)

TABLE I. Critical exponents η_{\parallel} , η_{\perp} , and y_{h_1} for the edge spin configurations of 2D coupled spin-dimer systems in Fig. 1.

terial [24]). The obtained estimates for y_{h_1} are listed in Table I and the scaling plots are shown in Fig. 3. For both edge spin configurations the critical exponents obey the above scaling relations to the precision of their estimated uncertainties.

We next consider the plaquette-square (PS) lattice [7, 35]; cf. Fig. 1(b). This model has been analyzed in the context of edge spin criticality in a recent publication [12], and we comment on the conclusions drawn by this work further below. Here, we consider PBC in the horizontal and open boundary conditions in the vertical direction; cf. Fig. 1(b). As a function of the coupling ratio J/J_D , this system shows two quantum critical points, at $J = J_{DAF} = 0.603520(10)J_D$ and for $J = J_{PAF} = 1.064382(13)J_D$. They separate the antiferromagnetic phase obtained for $J \approx J_D$ from the quantum-disordered dimer-singlet (plaquette-singlet) dominated phase for $J < J_{DAF}$ ($J > J_{PAF}$), respectively (we consider $J, J_D > 0$). Noting the difference between the two quantum-disordered phases with respect to the pattern of the predominant singlet formation, we distinguish the following four different edge spin configurations. (i) For $J < J_{DAF}$, the system is quantum disordered due to predominant singlet formation along the J_D dimer bonds, and thus the systems exhibits dangling spins if we cut through a row of dimers to obtain the bottom boundary in Fig. 1(b). At $J = J_{DAF}$, we hence denote this edge spin configuration as DAF-D. (ii) If for $J < J_{DAF}$ we instead consider the spins at the top edge in Fig. 1(b), we obtain nondangling spins and for $J = J_{DAF}$ we denote this edge spin configuration as DAF-N. (iii) For $J > J_{PAF}$, the system is instead quantum disordered due to predominant four-site singlet formation on the plaquettes formed by the J bonds, and the system thus exhibits dangling spins at the top edge in Fig. 1(b). At $J = J_{PAF}$, we thus denote this edge spin configuration as PAF-D. (iv) If for $J > J_{PAF}$ we instead consider spins at the bottom edge in Fig. 1(b), we obtain nondangling spins and for $J = J_{PAF}$ we denote this edge spin configuration as PAF-N. For the PS lattice, we can thus realize both the case of dangling and the nondangling edge spins at either quantum critical point by considering appropriate edges. The QMC data for the correlation function $C_{\parallel}(r)$ for both cases are also shown in Fig. 2. Performing again a finite-size scaling analysis of the correlation

functions $C_{\parallel}(L/2)$ and $C_{\perp}(L/2)$ as well as the staggered susceptibility χ_s of the edge spins (see Supplemental Material [24]), we obtain scaling exponents that essentially correspond to those for the other considered cases; cf. Table I and Fig. 3.

At the considered quantum critical points, which all belong to the 3D $O(3)$ universality class, the edge spins exhibit critical scaling exponents that apparently belong to two different classes, depending on whether the edge spins are dangling or not with respect to the predominant singlet formation in the neighboring quantum disordered phase [we find consistent exponents also for the square-lattice bilayer model with dangling (nondangling) edge spins (see Supplemental Material [24])]. For the nondangling case, the obtained critical exponent y_{h_1} is similar to the values $y_{h_1} = 0.813(2)$ and $y_{h_1} = 0.802(1)$ obtained from Monte Carlo [30] and conformal bootstrap [36] studies of the ordinary surface transition in the 3D $O(3)$ model, respectively. This is in accord with the expectation that the critical behavior for nondangling edge spins is induced by the quantum critical fluctuations of the bulk system. The estimated exponents are comparable even to the values $\eta_{\parallel} = 1.307$, $\eta_{\perp} = 0.664$ and $y_{h_1} = 0.846$, obtained for the ordinary surface transition from the second-order ϵ expansion of the $O(n)$ -symmetric vector model ($\epsilon = 4 - d$) [28, 37], after a déagagé evaluation at $\epsilon = 1$ and $n = 3$ [38]. Regarding the dangling case, one observes a similar closeness of the critical exponents to the values $\eta_{\parallel} = -0.445$, $\eta_{\perp} = -0.212$ and $y_{h_1} = 1.723$ obtained from second-order ϵ expansion for the special transition [28, 37], evaluated at $\epsilon = 1$ and $n = 3$ [38]; however, there is still some spread among the values in Table I and these estimates [39]. Moreover, as mentioned above, the 3D $O(3)$ model does not feature such a special transition, whereas the ϵ expansion is blind to this restriction [28]. To assess if this apparent similarity of the critical exponents extends beyond a mere coincidence or if fine-tuning is necessary, requires, e.g., an ϵ expansion in the presence of a θ term from the dangling edge spins, to be compared to the ϵ expansion for the classical special transition, evaluated at $n = 3$. We are not aware of such an argument.

In Ref. [12], the observation that the scaling exponents for the DAF-D configuration differ from the ordinary transition is argued to be a consequence of symmetry-protected-topological (SPT) order [40, 41] in the ground state for $J < J_{DAF}$ in the form of an Affleck-Kennedy-Lieb-Tasaki state [42]—in contrast to the trivial (non-SPT) nature of, e.g., the plaquette phase or the quantum-disordered phase of the CD model. However, we obtain such nonordinary exponents also in the PAF-D configuration at $J = J_{PAF}$ as well as for the critical CD model with dangling spins. The nonordinary edge criticality is thus not a characteristic feature of SPT phases but results from the dangling edge spin arrangement. Moreover, it is readily seen to be possible to adiabatically con-

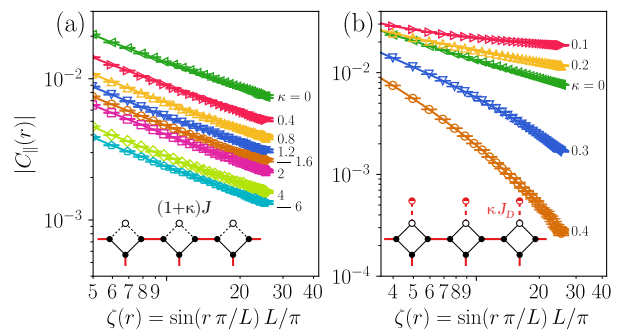


FIG. 4. (Color online) Lateral correlations $C_{\parallel}(r)$ vs. $\zeta(r)$ for the DAF-D configuration with different values of the edge coupling enhancement κ , as shown in the inset [left panel (a)], and for the DAF-D configuration with different values of the coupling κJ_D to additional spins, shown in the inset by semifilled circles [right panel (b)]. In both panels the curves are labeled by the value of κ .

nect the quantum-disordered phase of the PS model for $J < J_{DAF}$ to the quantum-disordered regime of the bilayer square lattice model without breaking any symmetries of the PS model (see Supplemental Material [24]).

In order to probe the stability of the scaling exponents with respect to variations of the edge spin couplings, we introduced modifications to the local environment of the dangling edge spins. We find that depending on the specific setting, different scenarios are realized. For example, enhancing the exchange couplings along the edge in the DAF-D configuration by a relative factor κ does apparently not significantly alter the critical properties of the edge spins; cf. Fig. 4(a). Its main effect is a uniform overall reduction of the correlations, such as if the increased couplings quench the magnetic moments on the edge sites by forming effective spin-1/2 moments on the \wedge -shaped outer triangles. On the other hand, coupling each dangling spin in the DAF-D configuration to an additional spin, as shown in the inset of Fig. 4(b), strongly affects the scaling of the original edge spin correlations: while for small values of the additional coupling κJ_D , the edge spin correlations increase, they are eventually suppressed at large values of κ , as shown in Fig. 4(b). This nonmonotonous behavior can be understood as follows: The additional couplings initially enhance antiferromagnetic tendencies, so that weak values of κ lead to more extended correlations. On the other hand, a further increase of κ leads to a predominant formation of local singlets on the new bonds, which eventually suppress the long-distance correlations. This perturbation, which allows us to tune from the DAF-D configuration ($\kappa = 0$) to the DAF-N configuration ($\kappa = 1$), thus exhibits explicitly the genuine quantum nature of these critical edge states. It may also be intriguing to examine the possibility of a true phase transition within the edge states along this line.

Based on the above findings, an analytical approach to the edge spin correlations in quantum critical bulk systems would be desirable, in particular in order to rationalize the apparent similarity of the exponents for the case of dangling spins with a naive extrapolation of the ϵ expansion for the special surface transition.

Note added. Recently, we became aware of a related study [38], where consistent numerical findings for the CD model are reported.

We thank F. F. Assaad, A. M. Läuchli, and T. C. Lang for useful discussions. F.P.T. is supported by the Deutsche Forschungsgemeinschaft (DFG) through Grant No. AS/120/13-1 of the FOR1807. SW and LW acknowledge support by the DFG through Grant No. WE/3649/4-2 of the FOR 1807 and through RTG 1995. Furthermore, we thank the IT Center at RWTH Aachen University and the JSC Jülich for access to computing time through JARA-HPC.

-
- [1] S. Sachdev, *Quantum Phase Transitions* (Cambridge University Press, Cambridge, 2011).
- [2] Ch. Rüegg, A. Furrer, D. Sheptyakov, T. Strässle, K. W. Krämer, H.-U. Güdel, and L. Mélési, *Phys. Rev. Lett.* **93**, 257201 (2004).
- [3] Ch. Rüegg, B. Normand, M. Matsumoto, Ch. Niedermayer, A. Furrer, K. W. Krämer, H.-U. Güdel, Ph. Bourges, Y. Sidis and H. Mutka, *Phys. Rev. Lett.* **95**, 267201 (2005).
- [4] Ch. Rüegg, B. Normand, M. Matsumoto, A. Furrer, D. McMorro, K. W. Krämer, H.-U. Güdel, S. Gvasaliya, H. Mutka, and M. Boehm, *Phys. Rev. Lett.* **100**, 205701 (2008).
- [5] P. Merchant, B. Normand, K. W. Krämer, M. Boehm, D. F. McMorro, and Ch. Rüegg, *Nature Phys.* **10**, 373 (2014).
- [6] J. Zinn-Justin, *Quantum Field Theory and Critical Phenomena* (Oxford University Press, Oxford, 2002).
- [7] M. Troyer, M. Imada, and K. Ueda, *J. Phys. Soc. Japan* **66**, 2957 (1997).
- [8] M. Matsumoto, C. Yasuda, S. Todo, and H. Takayama, *Phys. Rev. B* **65**, 014407 (2001).
- [9] Ling Wang, K. S. D. Beach, and Anders W. Sandvik, *Phys. Rev. B* **73**, 014431 (2006).
- [10] S. Wenzel, L. Bogacz, and W. Janke, *Phys. Rev. Lett.* **101**, 127202 (2008).
- [11] F.-J. Jiang, *Phys. Rev. B* **85**, 014414 (2012).
- [12] L. Zhang and F. Wang, *Phys. Rev. Lett.* **118**, 087201 (2017).
- [13] F. D. M. Haldane, ILL Report No. SP-81/95, 1981 (unpublished).
- [14] F. D. M. Haldane, *Phys. Rev. Lett.* **50**, 1153 (1983).
- [15] F. D. M. Haldane, *Phys. Lett. A* **93**, 464 (1983).
- [16] F. D. M. Haldane, *J. Appl. Phys.* **57**, 3359 (1985).
- [17] I. Affleck, *Nucl. Phys. B* **257**, 397 (1985).
- [18] I. Affleck, *Nucl. Phys. B* **265**, 409 (1985).
- [19] S. Chakravarty, B. I. Halperin, and D. R. Nelson, *Phys. Rev. Lett.* **60**, 1057 (1988).
- [20] S. Chakravarty, B. I. Halperin, and D. R. Nelson, *Phys. Rev. B* **39**, 2344 (1989).
- [21] A. V. Chubukov, S. Sachdev, and J. Ye, *Phys. Rev. B* **49**, 11919 (1994).
- [22] F. D. M. Haldane, *Phys. Rev. Lett.* **61**, 1029 (1988).
- [23] L. Fritz, R. L. Doretto, S. Wessel, S. Wenzel, S. Burdin, and M. Vojta, *Phys. Rev. B* **83**, 174416 (2011).
- [24] See the attached Supplemental Material for (i) the edge spin correlations for quantum-disordered dimerized bulk systems, (ii) the examination of finite-size effects in $C_{\parallel}(r)$ as a function of $\zeta(r)$, (iii) the finite-size scaling analysis of the bilayer square lattice models, (iv) further details of the finite-size scaling analysis, (v) the connection between the dimerized phases of the bilayer square lattice and plaquette-square lattice models.
- [25] T. Suzuki and M. Sato, *Phys. Rev. B* **86**, 224411 (2012).
- [26] K. Binder and P. C. Hohenberg, *Phys. Rev. B* **9**, 2194 (1974).
- [27] K. Binder, in *Phase Transitions and Critical Phenomena*, Vol. 8, edited by C. Domb and J. L. Lebowitz (Academic Press, London, 1983).
- [28] H. W. Diehl, in *Phase Transitions and Critical Phenomena*, Vol. 10, edited by C. Domb and J. L. Lebowitz (Academic Press, London, 1986).
- [29] N. D. Mermin and H. Wagner, *Phys. Rev. Lett.* **17**, 1133 (1966).
- [30] Y. Deng, H. W. J. Blote, and M. P. Nightingale, *Phys. Rev. E* **72**, 016128 (2005).
- [31] A. W. Sandvik and J. Kurkijarvi, *Phys. Rev. B* **43**, 5950 (1991).
- [32] A. W. Sandvik, *Phys. Rev. B* **59**, R14157 (1999).
- [33] P. Henelius, A. W. Sandvik, *Phys. Rev. B* **62**, 1102 (2000).
- [34] M. Campostrini, M. Hasenbusch, A. Pelissetto, P. Rossi, E. Vicari, *Phys. Rev. B* **65**, 144520 (2002).
- [35] M. Troyer, H. Kontani, and K. Ueda, *Phys. Rev. Lett.* **76**, 3822 (1996).
- [36] F. Gliozzi, P. Liendo, M. Meineri, A. Rago, *J. High Energ. Phys.* **2015**: 36 (2015).
- [37] H. W. Diehl and S. Dietrich, *Phys. Rev. B* **24**, 2878 (1981).
- [38] C. Ding, L. Zhang, and W. Guo, *Phys. Rev. Lett.* **120**, 235701 (2018).
- [39] Our estimated exponents for the DAF-D and PAF-N cases are consistent with those reported in Ref. [12]. Reference [12] also provides estimates of the critical exponents for a dangling edge spin configuration of the PS model at the quantum phase transition between the dimerized phase and the ferromagnetic regime at $J/J_D = -0.934251(11)$. The estimated values of the critical exponents, $\eta_{\parallel} = -0.561(4)$, $\eta_{\perp} = -0.2707(24)$ and $y_{h_1} = 1.7802(16)$ also differ slightly from the obtained values for the DAF-D case.
- [40] Z. C. Gu, and X.-G. Wen, *Phys. Rev. B* **80**, 155131 (2009).
- [41] X. Chen, Z.-C. Gu, Z.-X. Liu, and X.-G. Wen, *Science* **338**, 1604 (2012).
- [42] I. Affleck, T. Kennedy, E. H. Lieb, and H. Tasaki, *Phys. Rev. Lett.* **59**, 799 (1987).

SUPPLEMENTAL MATERIAL

Edge correlations for a quantum-disordered bulk

As an example of the effective spin-1/2 Heisenberg chain-like correlations that emerge at the edge of a quantum disordered bulk system, we show in Fig. S1 the lateral correlations $C_{\parallel}(r)$ (circles) as a function of the distance r between the edge spins for (i) the dangling edge spin configuration CD-D of the columnar dimer lattice (cf. the left inset), and (ii) the dangling edge spin configuration DAF-D of the plaquette-square lattice (cf. the right inset) for a coupling ratio of $J/J_D = 0.2$. For comparison, the corresponding correlation function of a spin-1/2 Heisenberg chain is also shown in this figure.

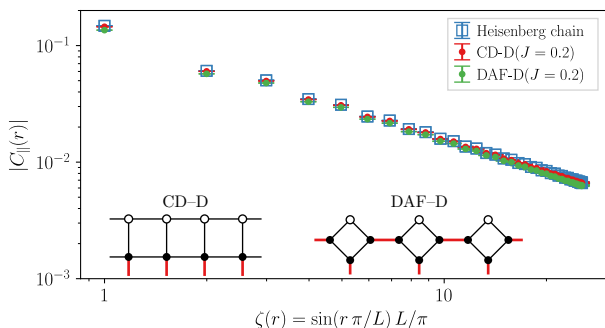


FIG. S1. Lateral correlations $C_{\parallel}(r)$ (circles) as a function of the cord distance $\zeta(r)$ between the edge spins for the two edge spin configurations shown in the insets: the dangling edge spin configuration CD-D of the columnar dimer lattice (left inset), and the configuration dangling edge spin DAF-D of the plaquette-square lattice (right inset), for a coupling ratio of $J/J_D = 0.2$, based on simulations with with $L = 80$, at a temperature of $T = 0.00125J_D$, and $T = 0.0003125J_D$, respectively. For comparison, the results of a spin-1/2 Heisenberg chain with 80 sites is also shown (squares).

Finite-size effects in $C_{\parallel}(r)$

Figure S2 shows the lateral correlations $C_{\parallel}(r)$ as a function of the conformal distance $\zeta(r)$ along the edge spins of the CD-N configuration shown in Fig. 1 of the main text for different values of the linear system size L .

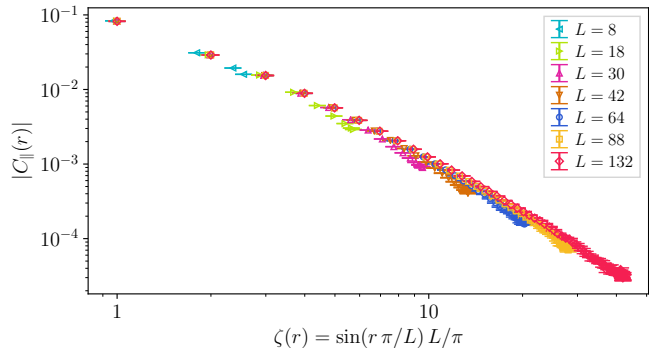


FIG. S2. Lateral correlations $C_{\parallel}(r)$ as a function of the conformal distance $\zeta(r)$ along the edge spins of the CD-N configuration shown in Fig. 1 of the main text for different values of the linear system size L . The temperature is scaled as $T = J_D/(2L)$ in all cases.

Configuration	η_{\parallel}	η_{\perp}	y_{h_1}
BS-N	1.32(8)	0.69(3)	0.87(2)
BS-D	-0.49(2)	-0.25(1)	1.733(3)

TABLE SII. Critical exponents η_{\parallel} , η_{\perp} , and y_{h_1} for the edge spin configurations of the bilayer square (BS) lattice in Fig. S3.

Results for the bilayer square lattice

In addition to the lattices discussed in the main text, we also investigate the bilayer square (BS) lattice. Here again, BS-D denotes the dangling and BS-N the nondangling edge configurations, cf. Fig. S3. The quantum critical point for the bilayer bulk system has previously been located at $J/J_D = 0.39651(2)$ [1]. The finite-size scaling of the QMC data for the lateral correlations $C_{\parallel}(L/2)$, the transverse correlatons $C_{\perp}(L/2)$, and the staggered susceptibility χ_s are given in Fig. S4. The critical exponents obtained from a fit to this data are given in Tab. SII and are consistent with the findings for the dangling and non-dangling edge spin configurations from the main text.

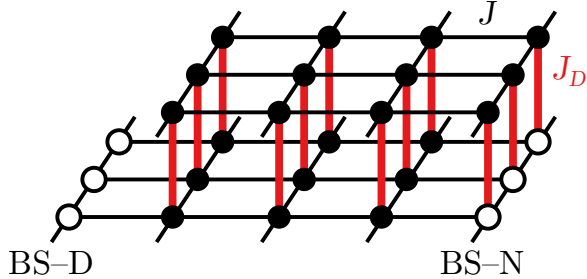


FIG. S3. BS lattice with dangling (BS-D) and nondangling (BS-N) edge spins. The J_D bonds (bold-red) here connect the two square lattice layers while the J bonds (black) form the intra-layer couplings. Open (full) circles denote the edge (bulk) spins.

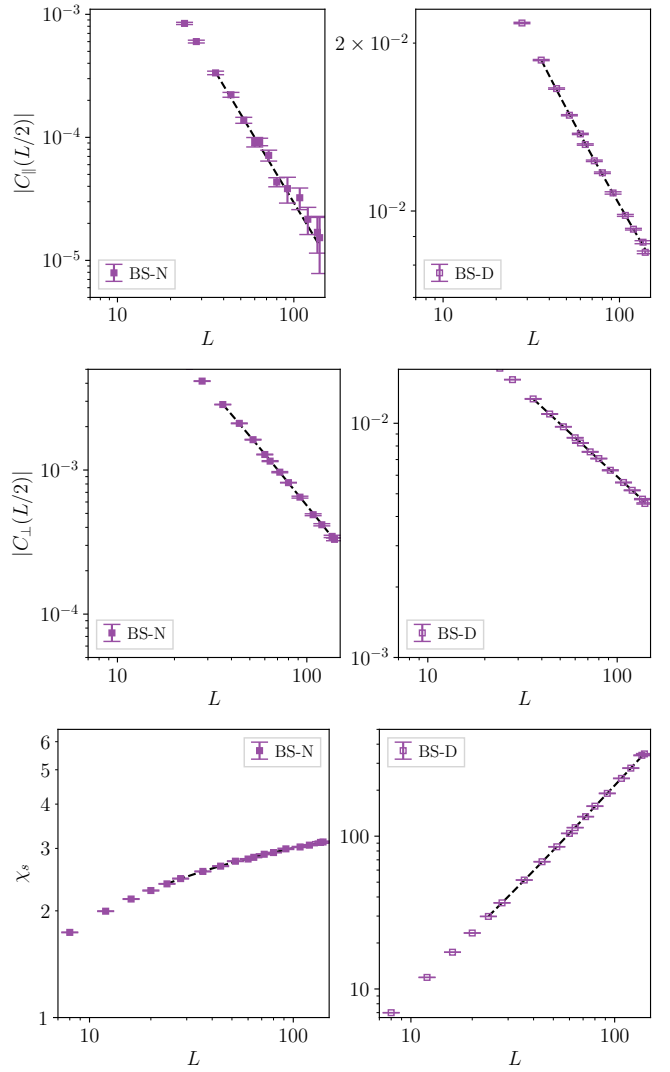


FIG. S4. $C_{\parallel}(L/2)$ (top panels), $C_{\perp}(L/2)$ (middle panels), and χ_s (bottom panels) as functions of L for the BS lattice edges shown in Fig. S3 along with finite-size fits (dashed lines).

Finite-size scaling analysis and scaling plots

Figure 3 of the main text shows the QMC data for the lateral correlations $C_{\parallel}(L/2)$, the transverse correlations $C_{\perp}(L/2)$, and the staggered susceptibility χ_s , as functions of L for the different edge spin configurations shown in Fig. 1 of the main text, along with fits corresponding to the finite-size analysis, based on the finite-size scaling ansatz given in main text. In the previous section of this supplemental material, we also present the corresponding QMC data for the BS lattice in Fig. S4 and the resulting exponents in Tab. SII.

Details concerning the range of system sizes from L_{\min} to L_{\max} that was accessible for the fitting procedure and whether inclusion of a scaling correction $c_1 L^{-1}$ and a nonsingular contribution c_{ns} was required, are provided for each specific case in Tab. SIII. In particular, a nonsingular contribution c_{ns} is required for extracting y_{h_1} from χ_s in the nondangling cases, because the exponent of χ_s is negative and thus the background is the dominating term, in contrast to the dangling cases, where χ_s diverges and the background term would be a sub-leading correction, compared to the leading scaling correction $\propto L^{-1}$. The L^{-1} correction term was included whenever a truncation of the interval from varying L_{\min} did not allow to compatibly fit the data to a simple power law. Also provided in Tab. SIII is the formula $N(L)$ for the number of lattice sites as a function of L for the various lattices.

Exponent	Config.	L_{\min}	L_{\max}	$N(L)$	$c_1 L^{-1}$ incl.	c_{ns} incl.
η_{\parallel}	CD-D	30	140	L^2	Yes	No
	BS-D	36	140	L^2	Yes	No
	DAF-D	18	88	$4L^2$	Yes	No
	PAF-D	18	88	$4L^2$	Yes	No
	CD-N	30	140	L^2	No	No
	BS-N	36	140	L^2	No	No
	DAF-N	18	88	$4L^2$	No	No
	PAF-N	18	88	$4L^2$	No	No
	η_{\perp}	CD-D	38	140	L^2	No
BS-D		36	140	L^2	Yes	No
DAF-D		18	88	$4L^2$	No	No
PAF-D		18	80	$4L^2$	No	No
CD-N		38	140	L^2	No	No
BS-N		36	140	L^2	Yes	No
DAF-N		18	80	$4L^2$	No	No
PAF-N		18	88	$4L^2$	No	No
y_{h_1}		CD-D	22	140	L^2	Yes
	BS-D	24	140	L^2	Yes	No
	DAF-D	14	88	$4L^2$	Yes	No
	PAF-D	14	88	$4L^2$	Yes	No
	CD-N	22	140	L^2	No	Yes
	BS-N	24	140	L^2	No	Yes
	DAF-N	14	88	$4L^2$	No	Yes
	PAF-N	14	88	$4L^2$	No	Yes

TABLE SIII. Details of the fitting range and fitting formula for the critical exponents η_{\parallel} , η_{\perp} , and y_{h_1} for the different edge spin configurations of 2D coupled spin-dimer systems.

We furthermore monitored the dependence of the extracted exponents on the minimum lattice size L_{\min} included in the fitting procedure. The dependence of the various critical exponents on L_{\min} is shown in Fig. S5. We observe no significant L_{\min} -dependence apart from strongly increasing uncertainties for the larger system sizes of L_{\min} , reflecting the fact that data from fewer system sizes are then available for the fitting procedure.

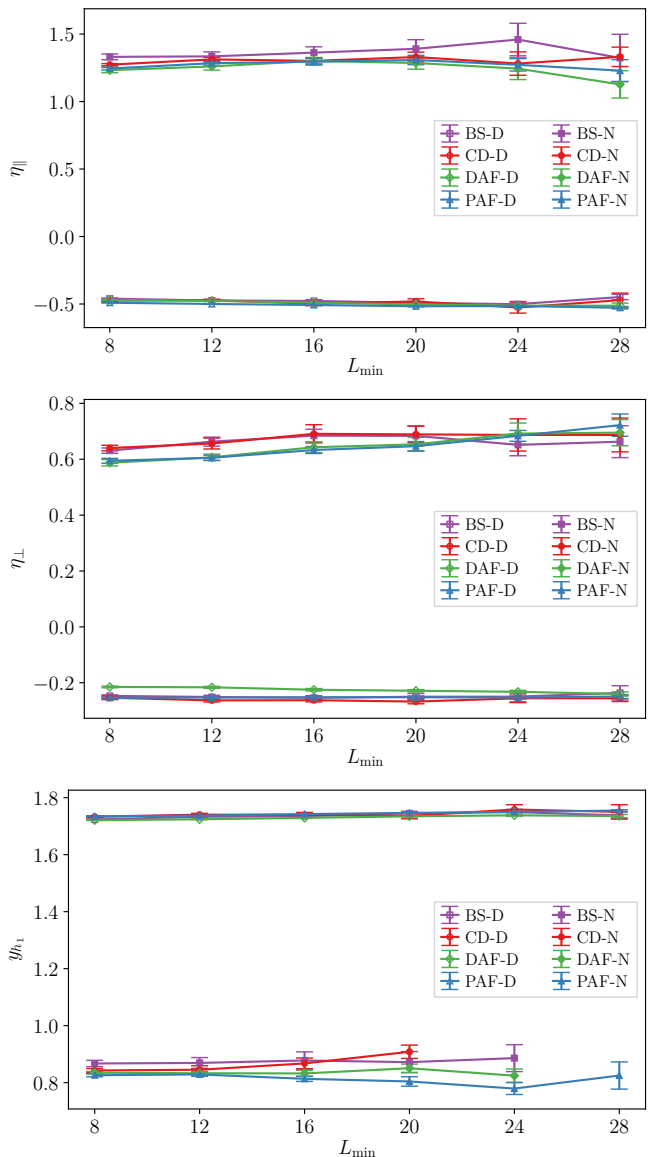


FIG. S5. Dependence of the estimate for η_{\parallel} (top panel), η_{\perp} (middle panel), and y_{h_1} (bottom panel) on the value of L_{\min} for the various considered edge spin configurations.

Finally, we also considered a finite-size scaling ansatz, wherein the scaling correction $\propto L^{-1}$ is replaced by a more general form $\propto L^{-\omega}$, with a free exponent ω . For example, $\omega \approx 0.8$ corresponds to the correction-to-scaling

exponent of the classical O(3) model at the 3D bulk phase transition [34]. As shown in Fig. S6, we observe only mild trends in the ω -dependence for some of the exponents. Anticipating the statistical uncertainties on the accessible system sizes, no significant qualitative changes result for the estimated exponents. Based on the above considerations, we thus consider the exponents given in Tab. I of the main text to provide reliable estimates for the current purpose of distinguishing the two different cases of dangling vs nondangling edge spin configurations.

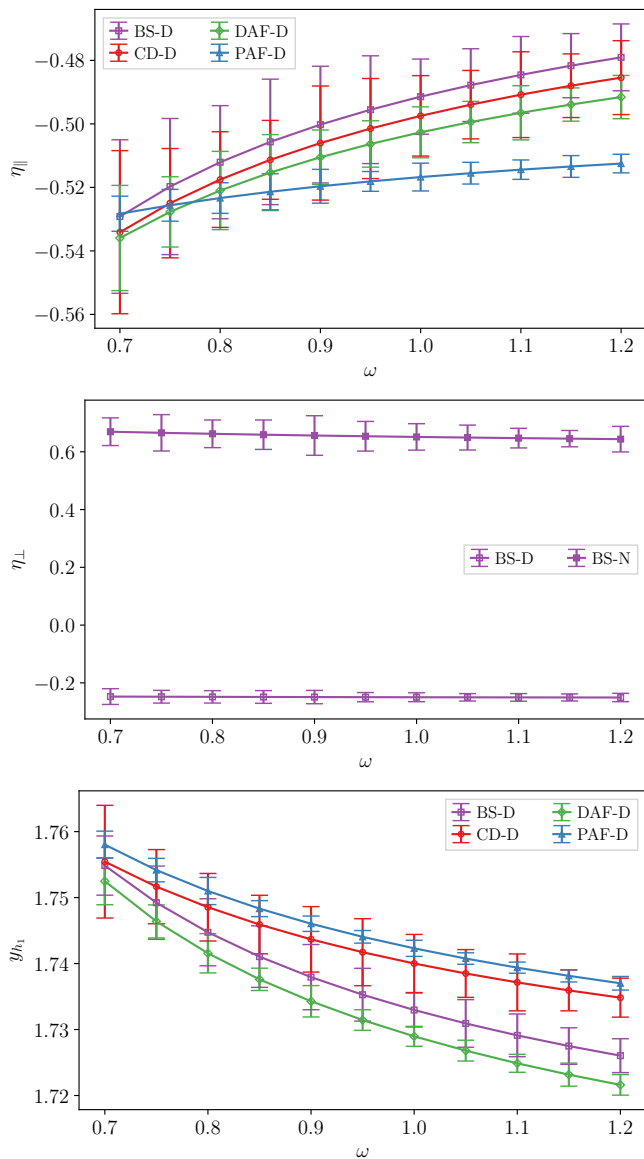


FIG. S6. Dependence of the estimate for η_{\parallel} (top panel), η_{\perp} (middle panel), and y_{h_1} (bottom panel) on the value of ω for the various considered edge spin configurations.

Connecting the plaquette-square and bilayer models

Figure S7 illustrates, how the bilayer lattice model is obtained from the plaquette-square lattice model upon increasing the additional exchange couplings J' from 0 to the value of J . During this process neither the internal SU(2) symmetry nor the spatial symmetries of the original plaquette square lattice are broken. The dimer bonds J_D thereby become the perpendicular inter-layer bonds. From explicit QMC calculations for different values of J/J_D inside the dimerized phase, one indeed obtains no indication for a quantum phase transition during this increase of J' , neither from the ground state energy nor the fidelity susceptibility. To relate to the more conventional presentation of the bilayer model, one may consider shifting all the blue (green) bonds and plaquettes up (down) to form the upper (lower) square lattice.

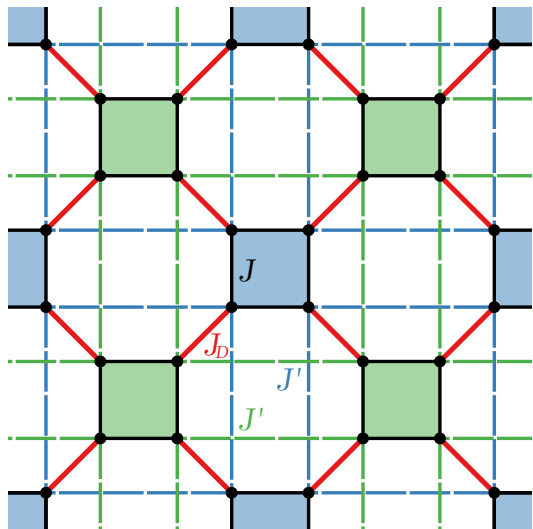


FIG. S7. Illustration showing how the bilayer square lattice is obtained from the plaquette-square lattice model upon increasing the couplings J' , indicated by dashed lines, from 0 to the value of J .

- [1] Ling Wang, K. S. D. Beach, and Anders W. Sandvik, Phys. Rev. B **73**, 014431 (2006).